Transverse instability of dunes

Eric J. R. Parteli[1,2], José S. Andrade Jr.[1], and Hans J. Herrmann[1,3]
1. Departamento de Física, Universidade Federal do Ceará - 60455-760, Fortaleza, Ceará, Brazil.
2. Programa de Pós-Graduação em Engenharia Química, Universidade Federal do Ceará, 60455-900, Fortaleza, Ceará, Brazil.
3. Computational Physics, IfB, ETH Zürich, Schafmattstr. 6, 8093 Zürich, Switzerland.

The simplest type of dune is the transverse one, which propagates with invariant profile orthogonally to a fixed wind direction. Here we show numerically and with a linear stability analysis that transverse dunes are unstable with respect to along-axis perturbations in their profile and decay on the bedrock into barchan dunes. Any forcing modulation amplifies exponentially with growth rate determined by the dune turnover time. We estimate the distance covered by a transverse dune before fully decaying into barchans and identify the patterns produced by different types of perturbation.

PACS numbers: 45.70.-n, 45.70.Qj, 05.65.+b, 45.70.Mg

Wind directionality and sand availability are the main factors dictating dune morphology. Bimodal and multidirectional wind systems form longitudinal and star dunes, respectively [1]. Under unimodal winds, two types of dune may occur, depending on the amount of sand: crescent-shaped barchans, evolving on the bedrock, and transverse dunes, which appear when the ground is covered with sand [1–3]. Studies of dune genesis have focused on the growth of longitudinal sand-wave instabilities of a plane leading to transverse dunes — which migrate downwind with invariant profile orthogonal to the transport direction [4]. The stability of the transverse dune shape, however, has remained a long-standing open issue, of relevance for several areas of aeolian research and planetary sciences. As shown in water tank experiments, a transverse sand ridge of finite length evolving on the bedrock destabilizes and decays into barchans when subjected to a stream of nearly constant direction [5].

The complete quantitative study of transverse dune evolution requires a mathematical modeling that combines the description of the average turbulent wind field with a model for sand transport in three dimensions [6–9]. Here we adapt this model in order to investigate systematically, for the first time, the stability of a transverse dune under unidirectional wind. The dune model consists of iteratively performing the calculations listed in the steps which follow.
(i) *Wind* — the average wind shear stress field ($\boldsymbol{\tau}$) over the terrain is calculated from the equation,

$$\boldsymbol{\tau} = |\boldsymbol{\tau}_0|(\boldsymbol{\tau}_0/|\boldsymbol{\tau}_0| + \hat{\boldsymbol{\tau}}), \tag{1}$$

where $\boldsymbol{\tau}_0$ is the wind shear stress over the flat ground, and the shear stress perturbation due to the local topography, $\hat{\boldsymbol{\tau}}$, is computed by solving the three-dimensional analytical equations of Weng *et al.* [10]. Since this wind model is only valid for smooth surfaces, the calculation must be adapted in order to account for flow separation at the dune brink. For each longitudinal slice of the dune, a separation streamline, $s(x, y)$, is introduced at the dune lee, where x and y are the directions longitudinal and perpendicular to the wind, respectively. The wind model is solved, then, for the envelope $h_s(x, y) = \max\{h(x, y), s(x, y)\}$ comprising the dune surface, $h(x, y)$, and the separation streamlines at the dune lee; these define the so-called separation bubble, inside which the wind shear is set to zero [7]. The shape of $s(x, y)$ is approximated by a third-order polynomial, the coefficients of which are calculated from the continuity of h, s and their respective first derivatives at the brink and at the reattachment point downwind, which is computed assuming that $s(x, y)$ has a maximum slope [7].
(ii) *Sand flux* — next, the mass flux of particles in *saltation* — which consists of grains travelling in ballistic trajectories and ejecting new particles upon collision with the bed [2] — is computed from a continuum model [6], in which the saltation cloud is regarded as a thin fluid-like layer moving over the immobile sand bed. When the wind shear stress exceeds a minimal threshold and saltation begins, the sand flux first grows exponentially due to the multiplicative process inherent to saltation transport. However, since the grains accelerate at cost of aeolian momentum, the flux cannot increase beyond a maximum value. This flux is reached after a saturation transient where the air shear stress within the saltation cloud equals the minimum value ($\tau_{\rm t}$) for sustained saltation [2, 11]. This mechanism of flux saturation is taken explicitly into account in the calculation of the height-integrated mass flux per unit length and time ($\boldsymbol{q}$),

$$\boldsymbol{\nabla}\cdot\boldsymbol{q} = (1 - |\boldsymbol{q}|/q_{\rm s})|\boldsymbol{q}|/\ell_{\rm s}, \tag{2}$$

where $q_{\rm s} = [2\alpha|\boldsymbol{v}_{\rm s}|/g](\tau - \tau_{\rm t})$ is the saturated flux, $\ell_{\rm s} = [2\alpha|\boldsymbol{v}_{\rm s}|^2/g\gamma]\tau_{\rm t}(\tau - \tau_{\rm t})^{-1}$ is the characteristic length of flux saturation, $\boldsymbol{v}_{\rm s}$ is the steady-state grain velocity, g is gravity, and $\alpha \approx 0.4$ and $\gamma \approx 0.2$ are empirically determined model parameters [6].
(iii) *Surface evolution* — the local height is updated from the equation,

$$\partial h/\partial t = -\boldsymbol{\nabla}\cdot\boldsymbol{q}/\rho_{\rm sand}, \tag{3}$$

where $\rho_{\rm sand}$ is the sand bulk density. Wherever the lo-

cal slope exceeds the static angle of repose of the sand ($\approx 34°$), the surface relaxes instantaneously through avalanches in the direction of the steepest descent [7]. Eq. (3) is then iteratively solved, using the flux of avalanches along the slip-face,

$$\boldsymbol{q}_{\rm aval} = k[\tanh(\nabla h) - \tanh(\theta_{\rm dyn})]\nabla h/|\nabla h|, \qquad (4)$$

where $k = 0.9$ and $\theta_{\rm dyn} = 33°$ is the dynamic angle of repose, until the local slope is below $\theta_{\rm dyn}$.

The calculations are performed with constant upwind shear stress (τ_0), and open and periodic boundaries in the directions x and y, respectively. First, a transverse sand ridge of Gaussian cross section and invariant profile orthogonally to the wind is let to evolve, under zero influx, into a transverse dune of height H and width L_0. The dune propagates, then, with fixed profile $h_0(x, y)$. The fragmentation of the dune into an array of barchans, reported from experiments [5], is not observed in the simulations. This result is independent of the amount of sand on the ground: the dune never breaks into barchans if $\tau_y = \partial h_0/\partial y = 0$, i.e. if the wind is unimodal and there is no variation in the transverse profile of the dune.

Next we add to the dune profile a small perturbation of the form $\hat{h}(y) = \delta_0\phi(y)$, where $\phi(y) = \cos[2\pi y/\lambda]$, with $\delta_0/H \ll 1$ and λ constant, such that the modified dune profile reads $h(x, y) = h_0(x, y) + \hat{h}(y)$. As shown in Fig. 1a, the perturbed dune is unstable, and decays after some time into a chain of barchan dunes, no matter the values of δ_0 or λ [12]. Differently from the behavior of transverse instabilities of flat granular surfaces forced by an initial modulation [13], there is no threshold wavelength for the growth of the perturbations. The transverse dune is unstable also when $\phi(y)$ is a random function of y (see Fig. 1a), or when the modulation is on the $xy-$plane.

The magnitude of the perturbation, $\delta(t)$, defined as the difference between the maximum and the mininum height measured along the dune crest, increases exponentially in time, $\delta(t) \sim \exp(\sigma t)$. The same behaviour is found for the difference between the maximum and minimum mass of longitudinal slices (Fig. 1b). No dependence on the parameters of the initial modulation is observed for the characteristic time scale $1/\sigma$ [12], which is found to decrease with the wind speed and to increase with dune size. From dimensional analysis, a scaling of σ with Q_0/H^2 is expected, where $Q_0 \equiv q_{\rm s}(\tau_0)/\rho_{\rm sand}$ is the saturated bulk sand flux associated with τ_0. The best fit to the simulation data leads to the expression (Fig. 1c),

$$\sigma \approx 0.32\, Q_0/H^2 = 1/T_{\rm m}, \qquad (5)$$

i.e. the time scale of the instability growth is in essence the turnover time, $T_{\rm m}$, of a barchan dune that has the same height H as the initial transverse dune [14].

In this manner, dune genesis involves two different kinds of sand-wave instabilities. The longitudinal one,

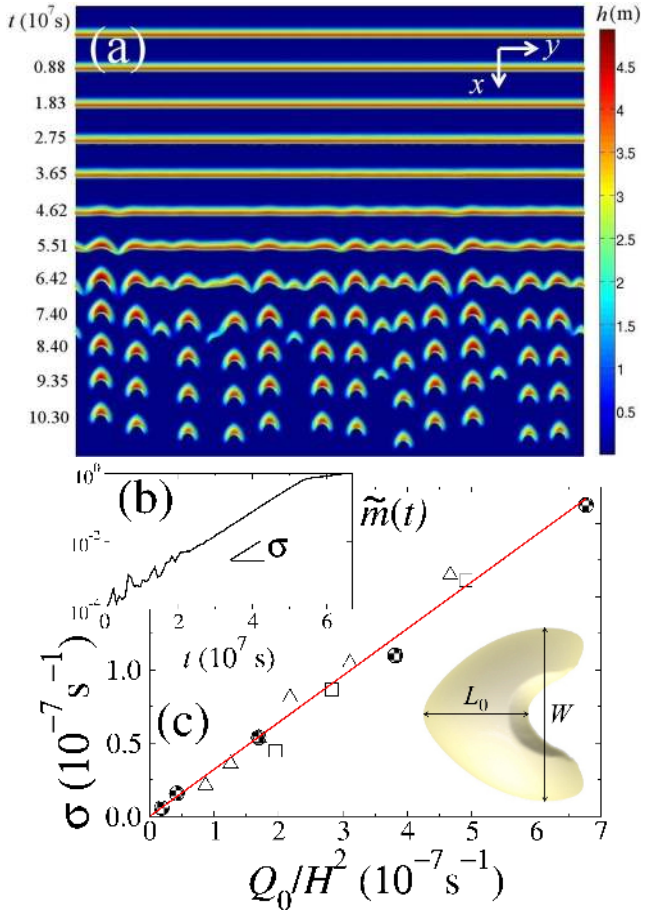

FIG. 1. **(a)** Spatio-temporal sketch showing the dune profile at different times plotted at the corresponding distance of migration downwind. Dune height is $H \approx 4.0$ m and the wind blows from the top with constant shear stress $\tau_0/\tau_{\rm t} \approx 3.1$. The initial perturbation is random with amplitude $\delta_0 = 12.5\mu$m, i.e. equal to the surface roughness (z_0), approximately 1/20 of a grain diameter [6]; the dune's turnover time is $T_{\rm m} \approx 6 \times 10^6$ s. **(b)** Time evolution of the modulation amplitude, $\tilde{m}(t) = 1 - M_{\rm min}/M_{\rm max}$, where $M_{\rm min}$ and $M_{\rm max}$ are, respectively, the minimum and maximum mass of the longitudinal slices at time t; $\tilde{m}(t)$ increases as $\exp(\sigma t)$. **(c)** σ scales with Q_0/H^2 (Eq. (5)). The continuous line, which has slope ≈ 0.32, is the best fit to the simulation data using Eq. (5). Circles: simulations with $\tau_0/\tau_{\rm t} \approx 2.6$ and 3 m $< H <$ 18 m; squares (triangles): $H = 4.0$ m (6.0 m) and $1.5 < \tau_0/\tau_{\rm t} < 6.0$. A simulated barchan, with central slice of length L_0 and corresponding cross-wind width W, is shown in the bottom right-hand corner.

which leads to the transverse dune [4, 7], results from the combined effect of an upwind shift of the shear stress with respect to topography and the downwind lag of sediment flux with respect to flow — the so-called saturation length ($\propto \ell_{\rm s}$), which is proportional to $\ell_{\rm drag}$, i.e. the grain diameter multiplied by the grain to fluid density ratio [6, 15]. The transverse instability, studied for the first time in the present work, is consequence of cross-

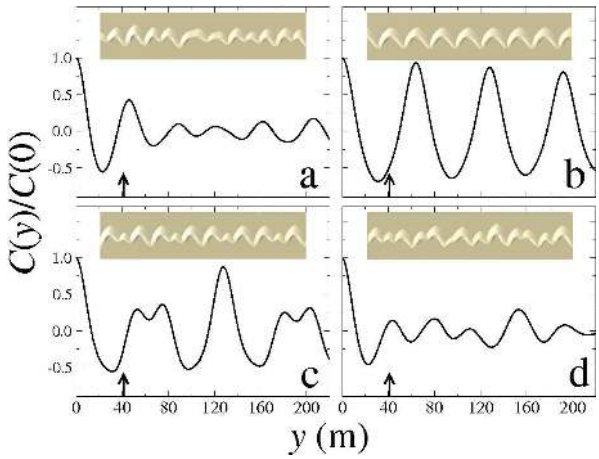

FIG. 2. Unstable patterns of a transverse dune of height $H = 3.0$ m under $\tau_0/\tau_t \approx 3.1$. Snapshots of simulations obtained with $\lambda = 4$ m (a), 64 m (b), 128 m (c) and random perturbation (d), all at $|\tilde{m}| \approx 99\%$. Each image has dimensions 512 m × 110 m. The plots show the corresponding auto-correlation functions $C(y) = \langle m(y+y')m(y')\rangle$ for the residual mass profiles $m(y,t) = M(y) - \langle M(y)\rangle$, where $M(y)$ is the mass of the $y-$th longitudinal slice and $C(0)$ is the square of the standard deviation. The first maximum of $C(y)$ gives the average wavelength. The arrow indicates the width ($W \approx 41$ m) of a barchan that has the same height as the transverse dune.

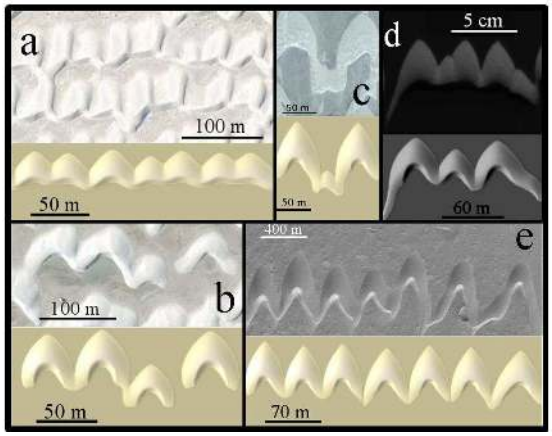

FIG. 3. Unstable dune patterns occuring in nature, together with the corresponding patterns obtained in the calculations. **(a,b)** dunes at White Sands and **(c)** Guerrero Negro, Baja California (images courtesy of Labomar); **(d)** barchans emerging from an unstable transverse dune in a water tank experiment [5] (image credit: Sylvain Courrech du Pont - Laboratoire MSC, Univ. Paris Diderot, Paris, France); **(e)** Martian barchans near 7.4°N, 292.3°W (image courtesy of NASA/JPL/MSSS).

wind sand transport along the dune axis, which plays a major role in coupling the longitudinal slices of dunes [2, 6]. We find from a linear stability analysis (see Section 2 of the Supplementary Material [12]) that, since different slices can have different velocities due to the relation $v \sim 1/H$, the lateral transport becomes the destabilizing factor for tranverse dunes.

In fact, when the perturbation is small and the lateral wind component is negligible, cross-wind transport occurs mainly due to gravitational downslope forces arising wherever on the slip-face the local slope exceeds the angle of repose [2, 7]. It can be easily verified that mass transfer between neighbouring slices occurs if there is a relative shift in their downwind positions: sand moves from the slices *advanced* downwind toward the retarded ones [12]. The relation $v \sim 1/H$ implies that the smaller slices, which migrate faster, move advanced with respect to the larger ones. Thus, if a small perturbation is applied to the mass profile of a transverse dune, then, due to lateral transport, the smaller slices lose mass and become even smaller and faster, while the larger slices become even larger and slower, such that the perturbation increases [12]. It can be shown that, in this linear regime (i.e. for small perturbation), the growth rate of the perturbation scales with $1/\lambda$ [12]. As the perturbation increases, nonlinear effects become important and the study of dune evolution must rely on numerical simulations (Fig. 1), which will be discussed next. If the dune is on the bedrock, then, when the perturbation becomes of the order of the dune height, barchans separate as sand is released through the emerging limbs along the barchanoidal chain.

The pattern of the emerging barchan chain depends on λ (Fig. 2). When λ is approximately $W \simeq 12H + 8\ell_{\rm drag}$ [9], i.e. the width of a barchan that has the same height (H) as the transverse dune, a nearly uniform chain of barchans emerges, all of width W. For larger λ the dune destabilizes in spatial cycles of wavelength λ, which, again, decay into smaller barchans. Periodicity is lost when $\lambda < W$ or when the perturbation is random. Nevertheless, at the time when barchans are about to separate, the characteristic wavelength of the unstable pattern in all cases is of the order of W, as can be seen in Fig. 2 from the auto-correlation function of the mass profile in transverse direction. Interestingly, simulations using the aforementioned parameters can qualitatively mimic different dune patterns found in Nature, as depicted in Fig. 3, suggesting that the patterns are quite generic. Our simulations show that all such patterns evolve toward an array of separated barchans, independently of the dune's past development stages or on the physical conditions.

From the expression $\delta(t) \approx \delta_0 \exp(t/T_{\rm m})$, it follows that a transverse dune of height H and profile modulated by a perturbation along the axis of initial amplitude δ_0 needs a time $T_\infty \approx T_{\rm m} \ln(H/\delta_0)$ to fully decay into barchans. The total length L_∞ covered by the transverse dune during the decay process should scale, thus, with $W \ln(H/\delta_0)$. Using the relation $W \approx c\, L_0$ (c.f. inset of Fig. 1c), where $c \approx 2.82 \cdot [0.88 - \tau_t/\tau_0]$ for $\tau_0/\tau_t > 2$ [12], we obtain $L_\infty \approx c L_0 \ln(H/\delta_0)$. Since δ_0 cannot be smaller than the

roughness of the sand surface (z_0), an upper bound for L_∞ can be estimated from the expression,

$$L_\infty \lesssim cL_0 \ln(H/z_0). \quad (6)$$

By assuming $z_0 \approx 10\mu$m [2, 16] and $c \approx 1.5$ [2, 3, 8, 17], a transverse dune with $H \approx 4$ m and $L_0 \approx 29$ m should fully break into barchans within a distance shorter than $L_\infty \approx 19L_0 \approx 550$ m. Since all information on wind speed and on the attributes of sediments and atmosphere are encoded in T_m and in the dune's morphological relations, Eq. (6) is universal, i.e. it can be used to predict L_∞ of a transverse dune under any physical condition.

In fact, the prediction of Eq. (6) is in agreement with observations from water tank experiments on transverse dunes moving under constant water stream (see Suppl. Mat. [12] for an image). In the experiments [5], a sand bar subjected to a flow of nearly constant direction is shaped into a transverse dune of height $H \approx 2$ mm and width $L_0 \approx 3$ cm. The dune destabilizes and gives rise to barchans, which separate after a distance $L_\infty \approx 3L_0$ [5]. Indeed, by taking $H = 2$ mm and the value $c = W/L_0 \approx 1$ of the barchans produced in the experiments [5], Eq. (6) predicts $L_\infty \lesssim 5.3\,L_0$, which is close but above the experimental value. Since in real conditions the initial perturbation δ_0 is normally larger than z_0 observed values of L_∞ should be, indeed, always smaller than the theoretical estimate (Eq. (6)). Moreover, varying wind directions are also a destabilizing factor and can further accelerate the decay process of transverse dunes [5, 17].

In summary, our results show that transverse dunes are unstable with respect to along-axis perturbations in their profile and decay into barchans if moving on the bedrock. Any instability amplifies with rate $1/T_\mathrm{m}$, whereas the cross-wind width of the emerging barchans scales with the dune height. Our calculations show that a transverse dune emerging, for instance, from a sand beach in a coastal area should, after reaching the bedrock, migrate only a few times its own width until decaying into a chain of barchans — indeed, small barchans can be observed already when the first dunes leave the sand beach and enter the bedrock area where the ground is not covered with sand [18]. These findings are clearly important to understand the mechanisms of dune size selection and the genesis and evolution of barchan dune fields.

The transverse instability explains why barchans are the dominant dune shapes in areas of low sand availability [2, 3]. Our linear stability analysis [12] in fact shows that any transverse dune is always unstable. Since the linear stability analysis cannot go beyond small deviations from the perfect translational invariance, it can not discriminate between a wavy shaped transverse dune with eventually propagating waves, a barchanoidal chain or a decomposition into individual barchans. So various scenarios might be possible if the ground is not a bedrock but mobile, wet or vegetated. This open question might be tackled in the future with large scale computations. Transverse dunes are in fact also unstable under variations in wind direction [5, 17] or collisions with other dunes [19]. While field observations are plagued with uncontrolled weather conditions and large time scales, it would be interesting to perform systematic laboratory experiments of the instability growth in order to confirm the results of our calculations.

We thank Sylvain Courrech du Pont for the images of his experiment and Orencio Durán for discussions. We also thank the Brazilian agencies CNPq, CAPES, FUNCAP, FINEP, and the CNPq/FUNCAP Pronex grant for financial support.

[1] R. J. Wasson and R. Hyde, Nature 304, 337 (1983).
[2] R. A. Bagnold, Physics of blown sand and desert dunes, Methuen, London, 289 pp. (1941).
[3] M. C. Bourke, *et al.*, Geomorphology 81, 440 (2006).
[4] J. F. Kennedy, Annu. Rev. Fluid Mech. 1, 147 (1969); J. D. Smith, J. Geophys. Res. 75, 5928 (1970); K. J. Richards, J. Fluid Mech. 99, 597 (1980); S. R. McLean, Earth-Science Rev. 29, 131 (1990); H. Yizhaq, N. J. Balmforth and A. Provenzale, Physica D 195, 207 (2004); A. Fourrière, P. Claudin and B. Andreotti, J. Fluid Mech. 649 287 (2010).
[5] E. Reffet, S. Courrech du Pont, P. Hersen and S. Douady, Geology 38, 491 (2010).
[6] G. Sauermann, K. Kroy and H. J. Herrmann, Phys. Rev. E. 64, 31305 (2001); O. Durán and H. J. Herrmann, J. Stat. Mech., P07011 (2006).
[7] K. Kroy, G. Sauermann and H. J. Herrmann, Phys. Rev. E. 66, 031302 (2002).
[8] G. Sauermann, *et al.*, Geomorphology 54, 245 (2003); E. J. R. Parteli and H. J. Herrmann, Phys. Rev. Lett. 98, 198001 (2007).
[9] O. Durán, E. J. R. Parteli and H. J. Herrmann, Earth Surf. Proc. Landforms 35, 1591 (2010).
[10] W. S. Weng, *et al.*, Acta Mechanica, Suppl. 2, 1 (1991).
[11] R. S. Anderson and P. K. Haff, Science 241, 820 (1988); M. P. Almeida, J. S. Andrade Jr. and H. J. Herrmann, Phys. Rev. Lett. 96, 018001 (2006); M. P. Almeida, E. J. R. Parteli, J. S. Andrade Jr. and H. J. Herrmann, Proc. Natl. Acad. Sci. 105, 6222 (2008); J. F. Kok, Phys. Rev. Lett. 104, 074502 (2010).
[12] see Supplementary Information.
[13] F. Malloggi, J. Lanuza, B. Andreotti and E. Clément, Europhys. Lett. 75, 825 (2006).
[14] J. R. L. Allen, Earth Sci. Rev. 10, 263 (1974); P. Hersen, *et al.*, Phys. Rev. E 69, 011304 (2004).
[15] P. Hersen, S. Douady and B. Andreotti, Phys. Rev. Lett. 89, 264301 (2002).
[16] D. J. Sherman and E. J. Farrell, J. Geophys. Res. 113, F02S08 (2008).
[17] H. Elbelrhiti, P. Claudin and B. Andreotti, Nature 437 (720).
[18] G. Kocurek, *et al.*, Journal of Sedimentary Petrology 62, 622 (1992); M. C. M. M. Luna, E. J. R. Parteli, O. Durán and H. J. Herrmann, Geomorphology 129, 215 (2011).
[19] P. Hersen and S. Douady, Geophys. Res. Lett. 32, L21403 (2005).

Supplementary Information

These supplementary notes are organized as follows:

- in section 1 we present auxiliary data, obtained from numerical simulations, that support the conclusions of the paper: (i) the growth rate of the instability does not depend on the amplitude of the initial perturbation; (ii) the ratio between the width (W) and the length of the central slice (L_0) of a barchan dune, i.e. $c = W/L_0$, is typically within the range $1 < c < 2$, provided the dune is well above the minimum size;
- a linear stability analysis of the transverse dune is presented in Section 2;
- in Section 3, we present experimental evidence of transverse dune instability.

1 The growth rate of the transverse instabilities does not depend on the amplitude of the initial perturbation

As mentioned in the paper, the rescaled difference between the maximum and the mininum mass of the dune's longitudinal slices, $\tilde{m} = 1 - M_{\rm min}/M_{\rm max}$, increases exponentially with time, i.e. $\tilde{m}(t) \propto \exp[\sigma t]$. The growth rate σ does not depend on the initial amplitude δ_0 of the perturbations, as illustrated in Fig. 1.

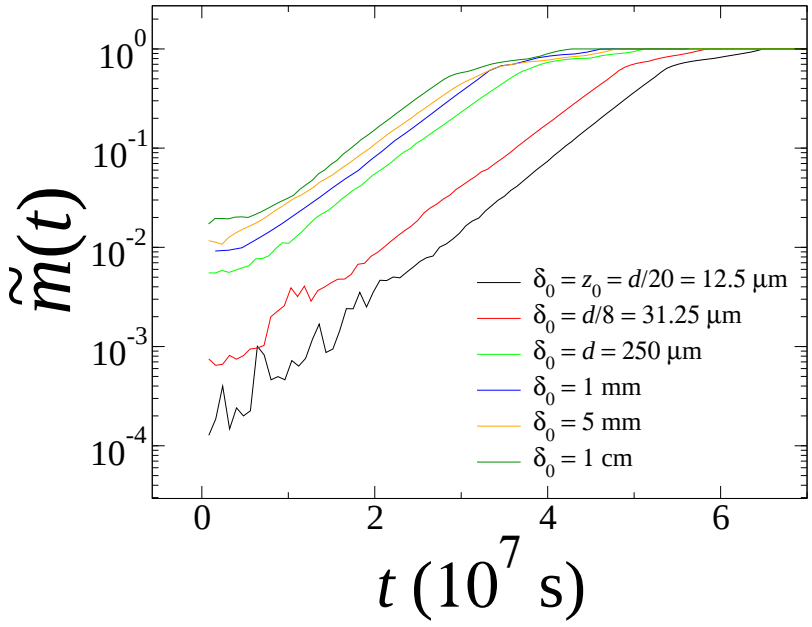

Figure 1: A random perturbation of amplitude τ_0 is applied to a transverse dune of height $H = 4.0$m under wind shear stress $\tau_0 \approx 3.1\tau_{\rm t}$. The time evolution of $\tilde{m}(t)$ is shown for different values of δ_0 ranging from the surface roughness z_0 up to values much larger than the grain diameter (d). We see that the growth rate $\sigma = {\rm d}(\log[\tilde{m}(t)])/{\rm d}t$ is independent of the value of δ_0.

Figure 1 refers to calculations using random perturbations of different initial amplitudes δ_0 applied to a transverse dune of height $H = 4.0$ m under shear stress $\tau_0 = 3.1\tau_{\rm t}$. As described in

the paper, the perturbed profile of the transverse dune at $t = 0$ reads $h(x, y) = h_0(x, y) + \delta_0\phi(y)$, where $h(x, y)$ is the undisturbed profile and $\phi(y)$ is a random function of y.

Indeed, the growth rate of the instabilities is a function of the dune size and the transport rate (Q_0) only. As discussed in the paper, we have fitted our simulation data using the equation $\sigma = aQ_0/H^2$, which led to the value $a \approx 0.32$. Therefore, $1/\sigma$ is in essence T_m, which is the turnover time of a barchan dune that has the same height, H, as the transverse dune. The turnover time, also called the reconstitution or migration time, is defined as the time a barchan dune needs to migrate a distance approximately equal to its width W. Since the dune migration velocity (v_m) scales as $v_\mathrm{m} \approx 50Q_0/W$ [1], $T_\mathrm{m} \approx W/v_\mathrm{m}$ can be estimated from the equation,

$$T_\mathrm{m} \approx \frac{W^2}{50Q_0}. \tag{1}$$

This equation can be written in terms of the dune height (H) by recalling that $W \approx 12H + 5$, which gives $T_\mathrm{m} \approx 3H^2/Q_0$. Therefore, the growth rate $\sigma = 1/T_\mathrm{m}$ scales with aQ_0/H^2, where the coefficient $a \approx 0.33$ is a value close to the one obtained from the fit to the simulation data (0.32).

From the equation for the exponential growth of the perturbation amplitude, we have also predicted in the paper the total length L_∞ covered by the transverse dune during the decay process. L_∞ is proportional to the decay time T_∞, and must scale, thus, with the dune turnover time T_m, which in turn scales with W, in such a manner that $L_\infty = W\ln[H/\delta_0]$. It is important to emphasize that W is not defined as the width of the emerging barchans (after the decay process), indeed barchans of different sizes emerge from the initial transverse dune. Rather, W is the width of a barchan that has the same height H as the initial transverse dune.

It is interesting to write L_∞ in terms of L_0, i.e. the width of the initial transverse dune, rather than in terms of W. However, L_0 does not follow a linear relation neither with H [2] nor with W. Instead, the ratio $c = W/L_0$ depends on the wind shear stress, as illustrated in fig. 2 (right). This figure shows that c is typically between 1 and 2, as mentioned in the paper, for typical values of shear stress (the wind shear velocity range shown in the figure is 0.27 m/s $< u_* <$ 0.50 m/s).

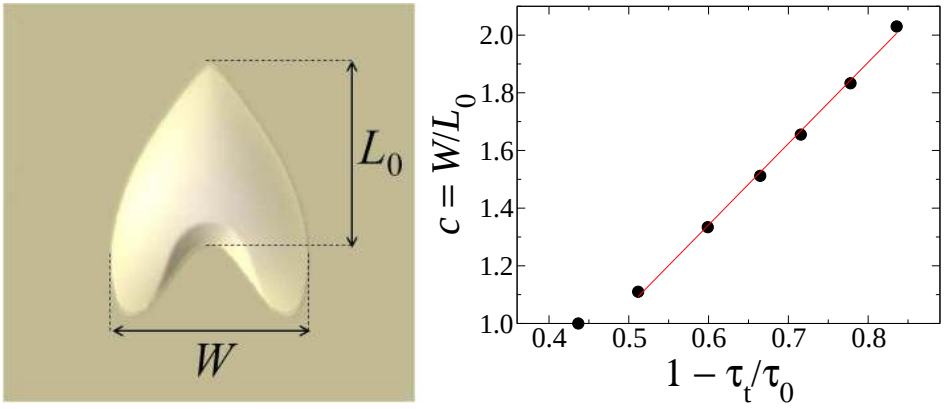

Figure 2: *Left*: A dune of height $H = 6.0$ m, shaped by an upwind shear stress $\tau_0 = 2.04\,\tau_\mathrm{t}$. The width ($W$) and the length of the central slice (L_0) of the dune are identified in the figure. *Right*: Ratio $c = W/L_0$ calculated for a dune $H = 16$ m for different values of the shear stress. The lower limit is $1 - \tau_\mathrm{t}/\tau_\mathrm{ft} = 0.36$, where $\tau_\mathrm{ft} = 1.25\tau_\mathrm{t}$ is the minimal threshold shear stress for direct entrainment [3, 4]. For large enough shear stress values, c increases approximately linearly with $1 - \tau_\mathrm{t}/\tau_0$ [2]; the best fit to the simulation data (red line) gives $c \approx 2.82 \cdot [0.88 - \tau_\mathrm{t}/\tau_0]$.

2 Stability analysis of the transverse dune

In this Section, our aim is to verify the transverse instability employing a linear stability analysis. Since we do not know the exact analytical form of the unperturbed solution, namely, the shape of the cross-section of the transverse dune in steady state, it is not possible to perform the full stability analysis of the three-dimensional transverse dune. However, we can simplify the problem by analyzing the perturbation at the dune's slip face, which is where the decisive transport mechanism takes place.

The physical picture behind our simplified analysis is that the speed of a very small slice of a transverse dune is essentially inversely proportional to its height (or more precisely to the square root of its area), since sand transport occurs only in a surface layer. So a perturbation on the area along the transverse direction will induce the smaller slices to move faster, while the larger ones stay behind. To assure the existence of an instability, it just suffices to show that there is a lateral flux of sand from advanced slices of the dune towards those that are behind, meaning that the smaller slices will become even smaller, and the larger ones even larger. Thus, their relative speed difference increases, therefore enhancing the perturbation. The most convenient place to perform this analysis seems to be the line in the front where the slip face reaches the ground, as we present in what follows.

Let us consider an infinite and flat transverse dune, moving under a wind in the x-direction that is strictly unidirectional. The mass of any infinitesimally longitudinal slice of this dune with width dy is given by $dM \approx \rho A dy$, where ρ is the bulk density of the dune, taken as a constant in our calculations. Considering that the slip face acts as a sand trap, the flux leaving a given slice in wind direction at the lee should be negligible. Thus, any change in the mass profile is due to mass exchange between neighbouring longitudinal slices, i.e., lateral transport along the y-axis. At time $t = 0$, we add to the area profile $A(y, t)$ of the dune an infinitesimal harmonic perturbation in y, i.e., in the direction orthogonal to the wind. In this manner, the perturbed area profile can be written as,

$$A(y, t) = A_0[1 + \epsilon \exp(\Lambda t) \cos(\omega y)], \tag{2}$$

where A_0 corresponds to the area of the unperturbed transverse dune, ϵ and ω are the initial amplitude and the frequency of the perturbation, respectively, and Λ is the growth rate of the perturbation. From Eq. (2), we see that the long-time behaviour of the perturbation is dictated by the sign of Λ. If $\Lambda < 0$, then the perturbation decreases and the transverse dune is stable. In contrast, a positive value of Λ makes the perturbation increase, which means that the transverse dune is unstable.

Imposing mass conservation, the time evolution of the area $A(y, t)$ of a given thin longitudinal slice can be obtained from,

$$\rho \frac{\partial A}{\partial t} = -\frac{\partial J}{\partial y}, \tag{3}$$

where $J(y, t)$ is the mass flux in units of mass per unit time, at position y and time t. At this point, we assume that the only relevant mechanism of mass transfer from one slice to a neighbouring one is the lateral transport induced by gravitational downslope forces, which arise at those areas where the local slope exceeds the angle of repose. Evidently such steep slopes only appear along the slip face at those longitudinal slices that are slightly advanced downwind. Indeed, such a longitudinal shift along the dune axis results if a perturbation of the form (2) is applied, because the migration velocity of a longitudinal slice increases with the inverse of its height — the smaller the slice, the faster its migration speed. Thus, the smaller slices migrate faster downwind with respect to their larger counterparts (see Fig. 3). In the present problem, the lateral flux can be written as

$$J = -B\rho A[s_{\max} - \tan(\theta_c)], \tag{4}$$

where B is a characteristic velocity for the avalanches on the slip face [1], $s_{\max}$ is the local slope in the steepest direction on the slip face, and $\theta_c = 34°$ is the angle of repose. As a first approximation,

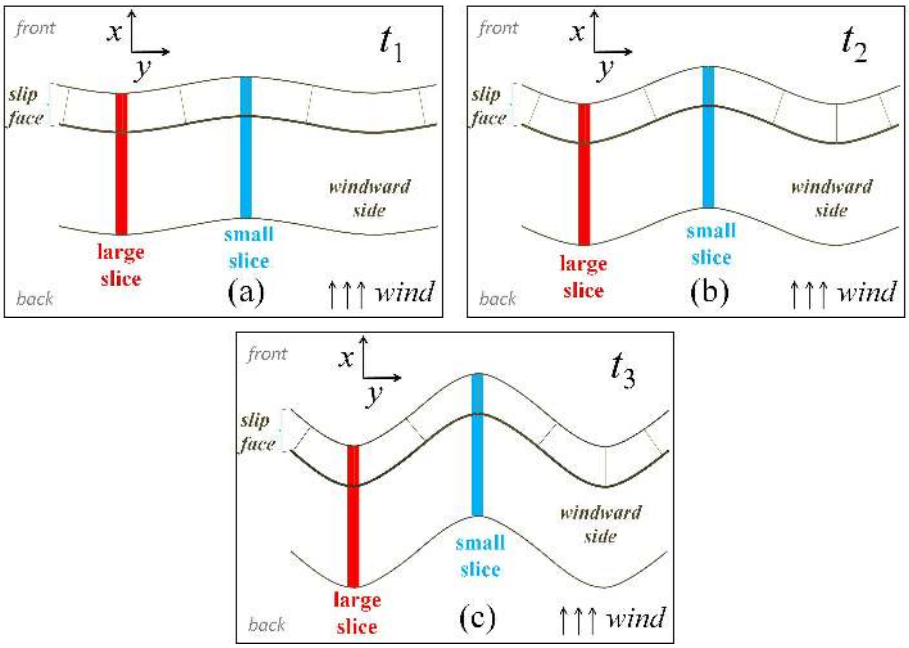

Figure 3: Schematic diagram illustrating the physical picture behind the analysis of the transverse dune instability. Figures (a), (b) and (c) show the projection of a transverse dune (viewed from the top), initially perturbed according to Eq. (2), at different instants of the evolution ($t_1 < t_2 < t_3$) — the analysis refers, of course, to the regime where the perturbation is very small, whereas in the figure the perturbation is shown exaggerated for clarity. Because different slices of the perturbed dune move with different velocities ($v \sim 1/H$ [3]), the periodic perturbation in the mass profile induces also a periodic phase shift in the position of the different slices (with respect to the wind direction). The smallest slices (indicated in blue) move faster downwind than the largest slices (red). Furthermore, the amplitude of the perturbation grows in time as sand is transferred from the smaller slices to the larger ones (c.f. Fig. 4).

here we assume that $s_{\max} \propto \frac{\partial h}{\partial y}$, where h is the local height of the dune.

Indeed, as already mentioned, lateral transport along the slip-face occurs from the advanced slices toward the retarded ones. The sketch displayed in Fig. 4 shows the longitudinal profiles at the lee of two dune slices of different heights, which have a relative shift of Δx in their respective downwind positions. At the slip-face's foot, the height of the dune surface at the more advanced slice is larger by an amount of $\Delta h = \tan(\theta_c)\Delta x$. Let us call $X(y,t)$ the longitudinal position of the slip-face's foot at slice y. From Fig. 4, we conclude that,

$$h(y,t) = \tan(\theta_c) X(y,t), \tag{5}$$

which, combined with Eq. (4), leads to

$$J(y,t) = -B\rho A \tan(\theta_c)(\frac{\partial X}{\partial y} - 1). \tag{6}$$

In order to determine the position $X(y,t)$, we use the fact that the migration velocity in the x-direction of a thin longitudinal slice follows the relation $v(y,t) = 2c/\sqrt{A(y,t)}$, where c is a constant which depends on the shear stress. Thus, the periodic perturbation in the area profile Eq. (2) induces a perturbation in the velocity of the form,

$$v(y,t) = \frac{2c}{\sqrt{A_0}}[1 + \epsilon \exp(\Lambda t)\cos(\omega y)]^{-1/2}. \tag{7}$$

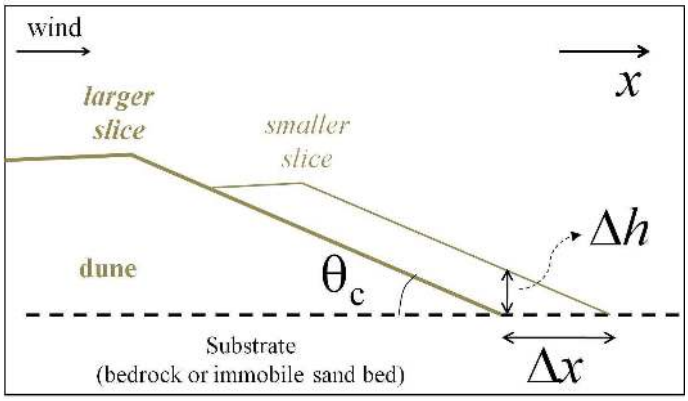

Figure 4: Sketch showing the longitudinal profiles of two neighbouring slices of a perturbed transverse dune. During an early time interval, when the perturbation is small, the smaller slice, which moves faster than its larger neighbour, advances by a relative distance Δx (in the figure, the perturbation is exaggerated for clarity). At the downwind position (x) corresponding to the slip-face's foot of the larger slice, the height of the dune surface at the smaller slice is larger by an amount of Δh. Therefore, during the initial phase of the perturbation growth, any transport along the axis occurring due to gravitational downslope forces occurs from the smaller (more advanced) slices to the larger (retarded) slices.

Since ϵ is small, this expression can be expanded in a Taylor series up to the first order in ϵ, such that $v(y,t)$ can be approximated to,

$$v(y,t) = \frac{2c}{\sqrt{A_0}}[1 - \frac{1}{2}\epsilon \exp(\Lambda t)\cos(\omega y)] + O(\epsilon^2). \tag{8}$$

The integration in time of Eq. (8) gives,

$$X(y,t) = X_0 + \frac{2c}{\sqrt{A_0}}t - \frac{c}{\Lambda\sqrt{A_0}}\epsilon \exp(\Lambda t)\cos(\omega y), \tag{9}$$

where X_0 is the initial position of the dune. Using Eq. (9) and the perturbation expression (2) to calculate $J(y,t)$ from Eq. (6), we can then apply mass conservation Eq. (3) to obtain the following identity:

$$A_0\epsilon\Lambda \exp(\Lambda t)\cos(\omega y) = A_0\epsilon B\tan(\theta_c)\frac{c\omega^2}{\Lambda\sqrt{A_0}}\exp(\Lambda t)\cos(\omega y) + O(\epsilon^2), \tag{10}$$

from which we can finally write,

$$\Lambda = \pm\omega\sqrt{\frac{B\tan(\theta_c)c}{\sqrt{A_0}}}. \tag{11}$$

Since the positive root in Eq. (11) dominates, we conclude that the perturbation should always grow in time. Our linear stability analysis corroborates, therefore, the results from our numerical simulations, namely, that transverse dunes are unstable with respect to perturbations along their axis.

It is important to emphasize that the growth rate Λ estimated in Eq. (11) refers only to the very initial stage of the evolution, where the perturbation can be considered to be small. As the amplitude grows and nonlinear effects become important, the growth rate is dictated by the dune's turnover time, whereas the most unstable mode is of the order of the cross-wind width (W) of a barchan that has the same height (H) as the transverse dune, as shown by our numerical simulations. It would be interesting to conduct a theoretical study of the instability growth that

incorporates in more detail nonlinear effects in order to compare with the predictions of our numerical simulations. However, a nonlinear stability analysis is beyond the scope of the present work.

Further, the stability analysis presented in this work does not distinguish between high and low sand amounts, i.e., the physical mechanisms driving the transverse instability exist also when transverse dunes evolve in areas of high sand availability, as for example on a dense sand bed. Evidently, however, if the amount of sand is sufficiently high the separation of the barchans does not occur — even though, transverse dunes are never straight, but always display a characteristic sinusoidal shape, which is a fingerprint of the intrinsic instability reported here. When the ground is covered with sand, sand exchange between dunes becomes a relevant factor for dune evolution and certainly plays a determinant role for the evolution of the instability. The evolution of the three-dimensional transverse dune shape under high sand amounts needs to be studied with systematic numerical simulations in the future.

3 Experimental evidence of transverse dune instability

The transverse dune instability studied in the present work has been confirmed in water tank experiments performed by Reffet *et al.* [5]. In these experiments, a transverse bar a few milimeters high (Fig. 5), which is submitted to a water stream of nearly constant direction, decays into a stream of barchans after a distance that is about 3 times its width. In this manner, our finding that transverse dunes are intrinsically unstable with respect to unimodal winds is consistent with the experimental observation. Furthermore, as discussed in the paper, our calculations predict the decay distance for the underwater dunes to be less than 5 times the dune width, and in this manner, the predictions of our simulations are consistent with the experimental observations. Figure 5 shows snapshots of the experiments [5] at different instants of the evolution.

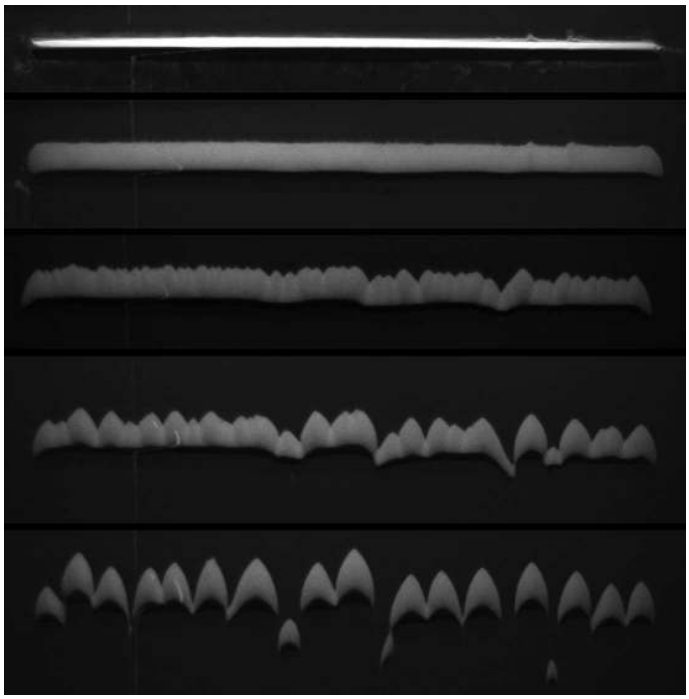

Figure 5: Water tank experiment [5]: A transverse dune submitted to a water stream of constant direction is unstable and decays into barchans. The direction of the stream is from top to bottom. The figure shows different snapshots of one experimental realization, at $t = 0$, 50, 200, 800 and 1600, respectively from the top to the bottom, where the "time" t is in fact an index, i.e. the number of the snapshot corresponding to the image [5]. In the experiment [5], an initial sand barrier ($t = 0$) evolves into a transverse dune of width ≈ 3 cm, which then migrates a distance of about 3 times its own width until decaying into barchans (which occurs after $t \approx 800$). Images are 56 cm wide. Images credit: Sylvain Courrech du Pont - Laboratoire MSC (Matière et Systèmes Complexes) - UMR 7057 - Université Paris Diderot, Paris, France.

References

[1] O. Durán, E. J. R. Parteli and H. J. Herrmann, Earth Surf. Process. Landforms **35,** 1591 (2010).

[2] K. Kroy, S. Fischer and B. Obermayer, J. Phys.: Condens. Matter **17,** S1229 (2005).

[3] R. A. Bagnold, *The physics of blown sand and desert dunes*, Methuen, London (1941).

[4] G. Sauermann, K. Kroy and H. J. Herrmann, Phys. Rev. E **64,** 31305 (2001).

[5] E. Reffet, S. Courrech du Pont, P. Hersen and S. Douady, Geology 38, 491 (2010).